SPE 39497

Capillary Pressure Correlation for Mixed-Wet Reservoirs

S.M. Skjaeveland, L.M. Siqveland, A. Kjosavik, Stavanger College, W.L. Hammervold, Statoil, G.A. Virnovsky, RF-Rogaland Research

This paper was prepared for presentation at the 1998 SPE India Oil and Gas Conference and Exhibition held in New Delhi, India, 10–12 February 1998.

Abstract

For waterwet reservoirs, several expressions may be used to correlate capillary pressure, or height above the free water level, with the water saturation. These correlations all feature a vertical asymptote at the residual water saturation where the capillary pressure goes to plus infinity.

We have developed a general capillary pressure correlation that covers primary drainage, imbibition, secondary drainage, and hysteresis scanning loops. The graph exhibits an asymptote at the residual saturation of water and of oil where the capillary pressure goes to plus and minus infinity, respectively. The shape of the correlation is simple yet flexible as a sum of two terms, each with two adjustable parameters and is verified by laboratory experiments and well-log data. An associated hysteresis scheme is also verified by experimental data.

The correlation can be used to make representative capillary pressure curves for numerical simulation of reservoirs with varying wettability and to model and interpret flooding processes.

Introduction

Many capillary pressure correlations have been suggested in the literature,[1–5] typically with two adjustable parameters. One parameter is expressing the pore size distribution and hence the curvature of the p_c-curve, the other the actual level of the capillary pressure, i.e., the entry or the mean capillary pressure.

Most of the correlations are limited to primary drainage and positive capillary pressures. Huang *et al.*[5] extend their correlation to include all four branches of the bounding hysteresis loop: spontaneous and forced imbibition, and spontaneous and forced secondary drainage. They employ the same primary drainage expression to each branch, scaled to render the measured $p_c = 0$ axis crossing.

We have chosen to base the general capillary pressure correlation for mixed-wet reservoir rock on the simple power-law form of Brooks and Corey[2,3] for primary drainage capillary pressure from $S_w = 1$ to S_{wr}. The classical expression for a waterwet core may be slightly rewritten to facilitate the extension of scope,

$$p_{cd} = \frac{c_{wd}}{\left(\frac{S_w - S_{wr}}{1 - S_{wr}}\right)^{a_{wd}}}, \quad \text{.....(1)}$$

where c_{wd} is the entry pressure, $1/a_{wd}$ the poresize distribution index,[6] S_{wr} the residual (irreducible) water saturation. The main reason for choosing this basis is the solid experimental verification of Eq. 1.[2,3]

According to Morrow,[7] there is now wide acceptance of the view that most reservoirs are at wettability conditions other than waterwet. To our knowledge, however, no comprehensive, validated correlation has been published for mixed-wet reservoirs. The lack of correlation makes it difficult to properly model displacement processes where imbibition is of importance and data are scarce, e.g., bottom water drive and water-alternate-gas injection.

In this paper, we present a general capillary pressure correlation and an associated hysteresis loop scheme. We try to demonstrate the applicability of the correlation by fitting data from a series of membrane and centrifuge experiments on fresh cores, and we show that the correlation is well suited to represent measured capillary pressure curves over a wide range of rock types. Also, analyzing well-log data from the same well in a bottom-water driven North Sea sandstone reservoir at several points in time over five years, we are able to model the transition from the initial primary drainage saturation distribution to the later observed imbibition profile.

The correlation crosses the zero capillary pressure axis at two points, for the imbibition and the secondary drainage branches. These points, together with the residual saturations, define the Amott-Harvey wettability index.[7] Thus, variations in wettability, e.g., with height, could be incorporated in the correlation.

We adopt the terminology of Morrow[7] to characterize the

capillary pressure curve, **Fig. 1**: 'drainage' denotes a fluid flow process where the water saturation is decreasing, even for an oilwet porous medium; 'imbibition' denotes a process where the oil saturation is decreasing; 'spontaneous' imbibition occurs for positive capillary pressure, 'forced' imbibition for negative capillary pressure; 'spontaneous' (secondary) drainage occurs for negative capillary pressure, and 'forced' (secondary) drainage for positive capillary pressure; 'primary' drainage denotes the initial drainage process starting from S_w = 1.0; and, for completeness, 'primary' imbibition denotes a imbibition process starting from $S_o = 1$.

Correlation

The design idea for the correlation is as follows: Eq. 1 is valid for a completely waterwet system and, if index *o* for oil is substituted for index *w*, it is equally valid for a completely oilwet system. For other cases between these limits, a correlation should be symmetrical with respect to the two fluids since neither dominates the wettability. One way to achieve a symmetrical form which is correct in the extremes, is to sum the two limiting expressions, i.e., to sum the water branch as given by Eq. 1 and a similar oil branch, resulting in the general expression,

$$p_c = \frac{c_w}{\left(\frac{S_w - S_{wr}}{1 - S_{wr}}\right)^{a_w}} + \frac{c_o}{\left(\frac{S_o - S_{or}}{1 - S_{or}}\right)^{a_o}} \quad \text{..... (2)}$$

The *a*'s and *c*'s are constants and there is one set for imbibition and another for drainage. An imbibition curve from S_{wr} to S_{or} is modeled by Eq. 2 and the four constants (a_{wi}, a_{oi}, c_{wi}, c_{oi}), and a secondary drainage curve from S_{or} to S_{wr} by the constants (a_{wd}, a_{od}, c_{wd}, c_{od}).

The constraints on the constants are that a_w, a_o, c_w are positive numbers and c_o is a negative number. The graph of Eq. 2, both for imbibition and drainage, therefore consists of two branches, a positive water branch with an asymptote at $S_w = S_{wr}$ and a negative oil branch with an asymptote at $S_o = S_{or}$, **Fig. 1**. Depicted in the figure are (1) the primary drainage curve starting at $S_w = 1$, modeled by Eq. 2 with $c_o = 0$ and c_w equal to the entry pressure; (2) the primary imbibition curve, from Eq. 2 with $c_w = 0$ and c_o equal to the entry pressure of water into a 100% oil saturated core; and (3) the bounding (secondary) imbibition and secondary drainage curves forming the largest possible hysteresis loop.

It should be noted that we have not performed any systematic study to check if the primary drainage constants c_{wd} and a_{wd} in Eq. 1 may have the same values as in the secondary drainage curve, Eq. 2 with the constants (a_{wd}, a_{od}, c_{wd}, c_{od}), or if two different sets of (a_{wd}, c_{wd}) are necessary. For simplicity, unless challenged by data, we will assume that a single set suffices.

For imbibition, the graph crosses the zero capillary pressure axis at S_{w0i}, i.e., $p_c(S_{w0i}) = 0$, giving the following expressions for c_{oi} from Eq. 2,

$$c_{oi} = -\frac{c_{wi}\left(\frac{1 - S_{w0i} - S_{or}}{1 - S_{or}}\right)^{a_{oi}}}{\left(\frac{S_{w0i} - S_{wr}}{1 - S_{wr}}\right)^{a_{wi}}}, \quad \text{.....(3a)}$$

and for secondary drainage, $p_c(S_{w0d}) = 0$, gives

$$c_{od} = -\frac{c_{wd}\left(\frac{1 - S_{w0d} - S_{or}}{1 - S_{or}}\right)^{a_{od}}}{\left(\frac{S_{w0d} - S_{wr}}{1 - S_{wr}}\right)^{a_{wd}}}. \quad \text{.....(3b)}$$

The wettability index to water, I_w, is given by[7] $I_w = (S_{w0i} - S_{wr})/(1 - S_{or} - S_{wr})$, and to oil, $I_o = (1 - S_{w0d} - S_{or})/(1 - S_{or} - S_{wr})$, and the Amott-Harvey wettability index[7] is $I_{AH} = I_w - I_o$. For a completely waterwet system, $I_w = 1$ and $I_o = 0$ giving $S_{w0i} = S_{w0d} = (1 - S_{or})$, and from Eq. 3, $c_{oi} = 0$ and $c_{od} = 0$. That is, Eq. 2 is used with only the water branch for both imbibition and drainage.

Wettability may vary with depth and be correlated with S_{wr}, as discussed by Jerauld and Rathmell.[8] Incorporating such variations into the capillary pressure correlation would require additional functional relationships between the parameters in Eqs. 3, e.g., if the reservoir becomes more waterwet as the water-oil contact is approached from above, both zeropoint crossings, S_{w0i} and S_{w0d}, should approach $(1 - S_{or})$, and c_{oi} and c_{od} go to zero. Also, if the interfacial tension is reduced for some displacement process, the *c*'s should go to zero proportionally, and S_{or} and S_{wr} should approach zero.

It could be considered to put Eq. 2 into dimensionless form by an extended *J*-function,[9] but it is not clear if this approach is valid for an imbibition process, as discussed by Hamon and Pellerin.[10] From their Fig. 8, it seems that the water branch of Eq. 2 could be scaled by the *J*-function, but that the oil branch is almost independent of permeability and would require a different scaling group.

Hysteresis Loop Logic

Introduction.

The hysteresis loop logic of Killough[11] is often employed in reservoir simulators. Its limitations have recently been discussed by Tan,[12] Kriebernegg and Heinemann,[13] and Kleppe *et al.*[14] who point out that Killough's method often is inadequate since it was formulated for the case where the drainage and imbibition curves meet at the residual oil saturation. To remedy the deficiency, it is suggested,[13,14] with some modifications,[14] to apply Land's[15] expression,

$$\frac{1}{S_{or}[1]} - \frac{1}{S_o[1]} = C, \quad \text{.....(4)}$$

where $S_o[1]$ is the start saturation of an imbibition process, on the primary drainage curve, and $S_{or}[1]$ is the end saturation of

the imbibition process, and C is Land's trapping constant.

A further limitation of Killough's procedure is that on the third reversal, an artificial jump back to the first reversal curve is made to ensure that the reversal scanning curves proceed back to the point where the original bounding curve was left, an experimental fact.

Design Constraints. We consider the following design constraints for capillary pressure hysteresis loops to be generally accepted based on experimental evidence:[16-20]

1. A first saturation reversal from the primary drainage curve, before reaching the residual water saturation S_{wr}, starts an imbibition scanning curve down to a residual oil saturation which is a certain fraction of S_{or}, as determined by Eq. 4.
2. If the reversal from the primary drainage curve occurs at S_{wr}, the scanning curve scans to S_{or} and is denoted the bounding imbibition curve.
3. A second reversal from S_{or} defines a (secondary) drainage bounding curve that scans back to S_{wr}. Together, the bounding imbibition and drainage curves constitute the closed bounding hysteresis loop.
4. All scanning curves originating on the bounding imbibition curve scan back to S_{wr}, and all reversals on the bounding drainage curve spawn scans back to S_{or}.
5. A scanning curve originating at $S_w[k]$, the water saturation at the start of the k'th reversal curve, will scan back to $S_w[k\text{-}1]$ and form a closed scanning (hysteresis) loop, unless a new reversal occurs.
6. If a curve scanning back from $S_w[k]$ reaches $S_w[k\text{-}1]$ before any new reversal, i.e., forms a closed scanning loop, the process continues by retracing the scan of the k-2 reversal as if the k-1 reversal had not occurred.
7. The shapes of the scanning loops are similar to the shape of the bounding loop.

Procedure. Let $S_w[k]$ denote the water saturation at the k'th reversal and let $[k]$ also label properties of the scanning curve after the k'th reversal with the convention that odd numbers denote imbibition and even numbers drainage. We will use the asymptotes $S_{wr}[k]$ and $S_{or}[k]$ as scanning loop residual saturations and S_{wr} and S_{or} as the bounding loop residual saturations.

First Reversal. The historic two-phase flooding process of a reservoir rock sample is usually primary drainage from $S_w = 1$. The first reversal will then be an imbibition curve denoted by $p_{ci}[1]$ originating from the primary drainage curve, $p_{cd}[0]$, Eq. 1. The reversal saturation $S_w[1]$ is a point on both the $p_{cd}[0]$ and the $p_{ci}[1]$ graph, that is

$$p_{cd}[0](S_w[1]) = p_{ci}[1](S_w[1]), \quad \text{.....(5a)}$$

and where explicitly, from Eqs. 1 and 2,

$$p_{cd}[0](S_w[1]) = \frac{c_{wd}}{\left(\frac{S_w[1]-S_{wr}}{1-S_w}\right)^{a_{wd}}}, \quad \text{.....(5b)}$$

$$p_{ci}[1](S_w[1]) = \frac{c_{wi}}{\left(\frac{S_w[1]-S_{wr}[1]}{1-S_{wr}[1]}\right)^{a_{wi}}} + \frac{c_{oi}}{\left(\frac{S_o[1]-S_{or}[1]}{1-S_{or}[1]}\right)^{a_{oi}}}. \quad \text{.....(5c)}$$

To honor Eq. 5a, we have to choose one parameter to be adjusted. Considering the design constraints, we keep all a's and c's constant for a given rock-fluid and adjust the water branch asymptote of the scanning curve, i.e., $S_{wr}[1]$. The oil branch asymptote, $S_{or}[1]$, is determined by Land's expression, Eq. 4. With this choice, the scanning curve will have a similar shape as the bounding imbibition curve since (a_{wi}, a_{oi}, c_{wi}, c_{oi}) are the same. The scanning curve may be considered to be part of a compression of the bounding imbibition curve between the two new asymptotes $S_{wr}[1]$ and $S_{or}[1]$.

In summary, the first reversal imbibition curve $p_{ci}[1](S_w)$ starts on the primary drainage curve at the reversal point $S_w[1]$ and scans down towards the asymptote $S_{or}[1]$, as shown in **Fig. 2** for three values of $S_w[1]$. Also shown in the figure is the bounding imbibition curve from S_{wr}, which is the minimum value of $S_w[1]$, back to S_{or}. All curves in the figure are produced with a constant set of parameters. Only the residual saturations (asymptotes) are varied. These manufactured curves nicely reproduce the features of the many experimental curves presented by Wardlaw and Taylor.[17]

Second Reversal From Residual Oil Saturation. The three (secondary) drainage scanning curves from the three $S_{or}[1]$-values and the bounding drainage curve from S_{or} are also shown in **Fig. 2**, forming 4 closed loops with their respective imbibition curves. The drainage scanning curves are generated by setting

$$p_{cd}[2](S_w[1]) = p_{cd}[0](S_w[1]), \quad \text{.....(6a)}$$

that is, the drainage curve following the second reversal, $p_{cd}[2]$, has to scan back to the first reversal point to make a closed loop. Here,

$$p_{cd}[2](S_w[1]) = \frac{c_{wd}}{\left(\frac{S_w[1]-S_{wr}[2]}{1-S_{wr}[2]}\right)^{a_{wd}}}$$

$$+\frac{c_{od}}{\left(\dfrac{S_o[1]-S_{or}[2]}{1-S_{or}[2]}\right)^{a_{od}}}, \quad \text{..... (6b)}$$

and $S_{or}[2] = S_{or}[1]$. The only unknown in Eq. 6a is then $S_{wr}[2]$, which can be calculated and the scanning curve is defined.

Second General Reversal. If a second reversal should occur at a point $S_w[2]$ on the $p_{ci}[1](S_w)$-curve, before reaching $S_{or}[1]$, a reversal drainage scanning curve, $p_{cd}[2](S_w)$, is spawned,

$$p_{cd}[2](S_w) = \frac{c_{wd}}{\left(\dfrac{S_w - S_{wr}[2]}{1-S_{wr}[2]}\right)^{a_{wd}}}$$

$$+\frac{c_{od}}{\left(\dfrac{S_o - S_{or}[2]}{1-S_{or}[2]}\right)^{a_{od}}}, \quad \text{..... (7)}$$

scanning back to $S_w[1]$. The imbibition scanning curve $p_{ci}[1]$ from $S_w[1]$ and the drainage scanning curve $p_{cd}[2]$ back again from $S_w[2]$ have to be equal at the two reversal points to form a closed loop, i.e.,

$$p_{ci}[1](S_w[1]) = p_{cd}[2](S_w[1]), \quad \text{.....(8a)}$$

and

$$p_{ci}[1](S_w[2]) = p_{cd}[2](S_w[2]). \quad \text{..... (8b)}$$

These two equations determine the two new asymptotes $S_{wr}[2]$ and $S_{or}[2]$ of $p_{cd}[2]$ in Eq. 7. As for the previous cases, we consider the a's and the c's to be invariant and adjust the vertical asymptotes of the scanning curve to get a closed loop. Thus the second scanning curve will be part of a compression of the secondary drainage curve between the two asymptotes $S_{wr}[2]$ and $S_{or}[2]$.

Numerically, Eqs. 8 can be solved as follows: Let the first estimate of $S_{wr}[2]$ be the previous value, $S_{wr}[1]$, and estimate $S_{or}[2]$ from Eq. 8a. With this estimate fixed, make a new estimate of $S_{wr}[2]$ from Eq. 8b, and flip-flop until convergence. Usually a couple of iterations is sufficient.

Third General Reversal. The $p_{cd}[2]$-process is now scanning from $S_w[2]$ and back to $S_w[1]$. If a new reversal occurs at $S_w[3]$ before reaching $S_w[1]$, a $p_{ci}[3]$-process is set up, scanning from $S_w[3]$ and back again to $S_w[2]$. If the $p_{cd}[2]$-process should reach $S_w[1]$, however, and the water saturation continues to decrease, the process reverts from a $p_{cd}[2]$-curve to a $p_{cd}[0]$-curve, i.e., it continues on the primary drainage curve.

More Reversals. The formalism can easily be generalized. **Fig. 3** shows another example of a set of enclosing scanning loops between the bounding curves. Let us say that the history started with a primary drainage from $S_w = 1$ to S_{wr}; then a first reversal, $S_w[1] = S_{wr}$, and the process traced the bounding imbibition curve until $S_w = 1 - S_{or}$, where the second reversal occurred, $S_w[2] = 1 - S_{or}$. Then the process followed the secondary drainage bounding curve until a third reversal at $S_w[3]$, the first reversal marked in the figure. The process now scans back on the $p_{ci}[3]$-curve towards $S_w[2]$ but experiences a fourth reversal at $S_w[4]$. Then two more reversals occur, $S_w[5]$ and $S_w[6]$. After the sixth reversal, the process scans back on the $p_{cd}[6]$-curve to $S_w[5]$, passes through this point, and continues on the p_{cd} [4]-curve back to $S_w[3]$ where it progresses on the $p_{cd}[2]$-curve, which, for this example, is the secondary drainage bounding curve.

Suite of Reversals From Bounding Curves. Several experimental papers[16,19] report series of reversals from the imbibition and drainage bounding loops with features described above in the design constraint No. 4. **Figs. 4 and 5** demonstrate that these features are well reproduced by the proposed hysteresis loop logic.

Bottom-Water Drive

The initial saturation distribution with height in a reservoir is usually determined by the primary drainage capillary pressure. When oil production starts, the Free Water Level [FWL]—the height where $p_c = 0$—slowly moves upwards. Each saturation in the capillary transition zone between oil and water becomes a reversal saturation $S_w[1]$ that spawns a scanning imbibition curve aiming at an $S_{or}[1]$-value given by Eq. 4. A sample calculation is shown in **Fig. 6**. Initially, the free water level is at height FWL_i. After it has risen to about 57 m, the saturation distribution follows an imbibition curve at low water saturations and exhibits a drainage-imbibition transition zone at high water saturations. This transition zone is a trapped feature that does not change as the water table continues to rise. The effect has been discussed by Kriebernegg and Heinemann.[13]

Validation

A capillary pressure correlation should have a minimum number of adjustable parameters yet be sufficiently flexible to fit a variety of measured datasets. Brooks and Corey[2,3] have shown that this is case for the water branch of Eq. 2, and we will try to validate the full form of Eq. 2.

Centrifuge Bounding Curve Data. Figs. 7 and 8 show the results of curvefitting the correlation to centrifuge data for two fresh core samples. The data are recorded from a forced imbibition and a forced secondary drainage process, i.e., half the water branch and half the oil branch are measured. This is a standard procedure by core laboratories. The curvefitting follows these steps:

1. When $S_w \to 1-S_{or}$, the oil branch dominates in Eq. 2, and a plot of $\log(-p_c)$ vs. $\log((S_o-S_{or})/(1-S_{or}))$ according to

$$\log(-p_c) = \log(-c_{oi}) - a_{oi}\log\left(\frac{S_o - S_{or}}{1-S_{or}}\right)$$

yields estimates of c_{oi} and a_{oi}. The lowest measured S_o-value is

used for S_{or}.

2. With no data available from spontaneous secondary drainage, we assume that $a_{od} = a_{oi} = a_o$, the inverse poresize distribution index at low oil saturations.

3. Since S_{w0i} is the known start saturation for forced imbibition, c_{wi} is found from Eq. 3a.

4. In the same manner are determined estimates of c_{wd} and a_{wd} from datapoints where $S_w \rightarrow S_{wr}$, and S_{wr} is set equal to the lowest measured water saturation, and c_{od} is found from Eq. 3a.

5. It is assumed that $a_{wd} = a_{wi} = a_w$, the inverse pore size distribution index in the low water saturation range.

6. With these estimates of the parameters, an expression for the total error is made by summing the errors squared between a measured capillary pressure and the correlation value, Eq. 2. The errors are weighted by the factor $(1/p_c)$.[2] The total error is simultaneously minimized with respect to a_o, a_w, c_{oi}, and c_{wd} by a standard optimization package, and c_{od} and c_{wi} are found by Eqs. 3.

The match in **Figs. 7 and 8** is good, which is also the case for all the other centrifuge results we have investigated.

Micropore Membrane Loop Data. We have matched a reported[18] series of capillary pressure experiments on a fresh, oilwet reservoir core to further check the applicability of the correlation and the hysteresis loop logic.

The core was not cleaned. It was saturated with dead crude oil and formation water and the last preparatory flow was a waterflood until no more oil was produced. Then the experiment followed this sequence (capillary pressures in millibar, mb):

(a) drainage to +350 mb
(b) spontaneous imbibition, +350 → +1 mb
 - bounding curve
(c) forced imbibition, 0 → –350 mb
 - bounding curve
(d) spontaneous drainage, –350 → –1 mb
 - bounding curve
(e) scanning loop, –1 → –5 → –1 mb
 - small
(f) scanning loop, –1 → –10 → –1 mb
 - medium
(g) scanning loop, –1 → –20 → –1 mb
 - large
(h) forced drainage, 0 → +350 mb
 - bounding curve.

In measurement series (a), an attempt was made to drive the system to S_{wr} to ensure that the rest of the steps are all within the bounding hysteresis loop.

First we fitted the bounding curves as described above for the centrifuge data, assuming $a_{wi} = a_{wd}$ and $a_{oi} = a_{od}$. This gave a reasonably good overall match with some discrepancy for measurement series (d). The fit improved when the a's for drainage and imbibition were allowed to be different. Still, the match for the drainage part of the scanning loops could have been better. Since, by assumption, the a's and c's are the same for all the curves, we decided instead to match the largest scanning loop and predict the medium and small scanning loops and the bounding loops.

The final match for the large scanning loop is shown in **Fig. 9**, the predicted medium loop in **Fig. 10**, and the predicted small scanning loop in **Fig. 11**. All three scanning loops and the measured data are shown together in **Fig. 12**. The scanning drainage curves for the medium and small loops are predicted by the hysteresis loop logic explained above. The only adaption is the choice of reversal points for the start of the drainage curves of the medium and small loops. In **Fig. 13** are shown the predicted bounding curves together with the measured data and **Fig. 14** summarizes the bounding and scanning curves together with the measured data. Although further fine tuning could have been performed and the data contain some drift due to the ramping speed,[18] the capillary pressure correlation and the hysteresis loop logic model the experiments satisfactorily.

Well Log Data From a Bottom-Water Driven Reservoir. In **Fig. 15** is shown a plot of height above the free water level vs. water saturation for a well from a sandstone reservoir in the North Sea. The data are logged in 1989 before the reservoir was put on production and follow a primary drainage drainage curve, Eq. 1. Data from tight shale stringers have been deleted from the match and J-function normalization has not been attempted.

After production start, the well was logged again in 1992, 1993, and 1994. The signal-to-noise ratio is worse for the completed well. In 1994, the FWL had risen about 85 meters and the portion of data above the transition from primary drainage to imbibition may be fitted with a pure imbibition curve. The result is shown in **Fig. 16**, where all the datapoints have been included, also those "masked" while matching. The position of the FWL is now an additional matching parameter. From knowledge of the residual saturations S_{wr} and S_{or} from the match, Land's trapping constant was determined from Eq. 4.

With all parameters fixed except FWL, which was adjusted separately, the saturation distribution with height was predicted by the capillary pressure correlation for the 1992 data in **Fig. 17** and the 1993 data in **Fig. 18**, all datapoints included. Although there is a wide spread in the data, and the matching procedure surely could be improved, the correlation fairly well predicts the rise of the water table.

Relative Permeability Functions

The Corey-type[6] or powerlaw expressions are popular correlations for relative permeabilities of waterwet reservoirs. They may be predicted from the primary drainage capillary pressure curve or fitted to measured relative permeability values. It seems reasonable that an extension to mixed-wet reservoirs would require a symmetrization with respect to the two fluids, possibly along the following lines:

Let k_{rwwd} denote the drainage relative permeability to water in a completely waterwet system, i.e., derived solely from the water branch of the general capillary pressure correlation,

Eq. 2, and let k_{rowd} denote the corresponding oil relative permeability. Then the Corey-Burdine[6,21] expressions are

$$k_{rwwd} = S_{nw}^{3+2a_{wd}}\ ,\ k_{rowd} = (1 - S_{nw}^{2a_{wd}+1})(1 - S_{nw})^2\ ,$$

where

$$S_{nw} = \frac{S_w - S_{wr}}{1 - S_{wr} - S_{or}}\ ,$$

for secondary drainage and with S_{or} dropped for primary drainage.

For a completely oilwet system, solely from the oil branch of the capillary pressure correlation, we may write for the oil and water relative permeabilities, respectively

$$k_{rood} = S_{no}^{3+2a_{od}}\ ,\ k_{rwod} = (1 - S_{no}^{2a_{od}+1})(1 - S_{no})^2\ ,$$

where

$$S_{no} = \frac{S_o - S_{or}}{1 - S_{wr} - S_{or}}\ .$$

For a mixed-wet system, the water phase could be perceived to move partly as a wetting phase and partly as a nonwetting phase with relative strengths c_{wd} and c_{od}, the weight factors on the water and oil branches of the capillary pressure correlation, Eq. 2, implying the following expression for the drainage water relative permeability of the mixed-wet system,

$$k_{rwd} = \frac{c_{wd}k_{rwwd} - c_{od}k_{rwod}}{c_{wd} - c_{od}}\ , \quad \text{.....(8a)}$$

and

$$k_{rod} = \frac{c_{wd}k_{rowd} - c_{od}k_{rood}}{c_{wd} - c_{od}}\ , \quad \text{..... (8b)}$$

for the drainage oil relative. Of course, Eqs. 8 represent just an educated guess of the shape of the correlations. Validation and possible modifications are needed based on consistent measurements of capillary pressure and relative permeability functions. For instance, endpoint relative permeability values at residual saturations for each of the Corey-Burdine expressions could be introduced as a modification.

A relative permeability hysteresis loop logic should be designed to honor measurements[22] and be consistent with the capillary pressure hysteresis loop logic.

As examples, **Figs. 19 and 20** show three pairs of relative permeability curves for oil and water: (1) primary drainage, (2) imbibition, and (3) secondary drainage. The a and c parameters in Eqs. 8 and the corresponding expressions for imbibition are taken from the capillary pressure correlation fit to the centrifuge data in **Figs. 7 and 8.**

Conclusions

1. A general capillary pressure correlation for mixed-wet rock is presented and its applicability demonstrated.
2. An new hysteresis scanning loop scheme is developed and validated by comparison with measurements.
3. The hysteresis scheme is employed to model the transition of the vertical saturation distribution in a reservoir from an initial primary drainage curve to an imbibition curve as the water table rises.
4. An extension of the Corey-type relative permeability correlation is suggested for mixed-wet rock.

Nomenclature

a = constant, dimensionless
c = constant, bar or mbar
k_r = relative permeability, dimensionless
p = pressure, bar or mbar
C = Land's trapping constant, dimensionless
I = wettability index
S = saturation
$[k]$ = scanning loop reversal No. k

Subscripts

c = capillary
d = drainage
i = imbibition or initial
n = normalized
o = oil or oilwet
r = residual or relative
w = water or waterwet
AH = Amott-Harvey
0 = zero point ($p_c = 0$)

Acronyms

FWL= Free Water level

Acknowledgements

We thank Den norske stats oljeselskap a.s. (Statoil) for support and permission to publish the paper.

References

1. Bentsen, R.G. and Anli, J.: "Using Parameter Estimation Techniques To Convert Centrifuge Data Into a Capillary-Pressure Curve," *SPEJ* (Feb. 1977) 57–64; Trans., AIME (1977) **263**.
2. Brooks, R.H. and Corey, A.T.: "Hydraulic Properties of Porous Media," Hydraulic Paper No. 3, Colorado State University, 1964.
3. Brooks, R.H. and Corey, A.T.: "Properties of Porous Media Affecting Fluid Flow," *J. of the Irrigation and Drainage Division, Proc. of ASCE*, **92**, No. IR2, (1966) 61–88.
4. Parker, J.C. and Lenhard, R.J.: "A Model for Hysteretic Constitutive Relations Governing Multiphase Flow, 1. Saturation-Pressure Relations," *Water Resources Research,* **23,** No. 12, (1987) 2187–2196.
5. Huang, D.D., Honarpour, M.M., and Al-Hussainy, R.: "An Improved Model for Relative Permeability and Capillary Pressure Incorporating Wettability," paper presented at the 1997 Society of Core Analysts International Symposium, Calgary, Sept. 7–10.
6. Standing, M.B.: "Notes on Relative Permeability Relationships," unpublished report, Department of Petroleum Engineer-

ing and Applied Geophysics, The Norwegian Institute of Technology, The University of Trondheim, Aug. 1974.
7. Morrow, N.R.: "Wettability and Its Effects on Oil Recovery," *JPT* (Dec. 1990) 1476–1484; *Trans.*, AIME, **289**.
8. Jerauld, G.R. and Rathmell, J.J.: "Wettability and Relative Permeability of Prudhoe Bay. A Case Study of Mixed-Wet Reservoirs," *SPERE* (Feb. 1997) 58–65.
9. Leverett M.C.: "Capillary Behaviour in Porous Solids." *Trans*. AIME (1941) **142**, 159–72.
10. Hamon, G. and Pellerin, F.M.: "Evidencing Capillary Pressure and Relative Permeability Trends for Reservoir Simulation," paper SPE 38898 presented at the 1997 SPE Annual Technical Conference and Exhibition, San Antonio, Oct. 5–8.
11. Killough, J.E.: ``Reservoir Simulation with History-Dependent Saturation Functions," *SPEJ* (Feb. 1976) 37–47; *Trans.,* AIME, **261.**
12. Tan, T.: "Representation of Hysteresis in Capillary Pressure for Reservoir Simulation Models," *J. Cdn. Pet. Tech.* (July-Aug. 1990) **29**, 4, 84–88.
13. Kriebernegg, M. and Heinemann, Z.: "A New Model for History Dependent Saturation Functions in Reservoir Simulation," paper presented at the 1996 European Conference on the Mathematics of Oil Recovery, Leoben, Austria, Sept. 3–6.
14. Kleppe, J., Delaplace, P., Lenormand, R., Hamon, G., and Chaput, E.: "Representation of Capillary Pressure Hysteresis in Reservoir Simulation," paper SPE 38899 presented at the 1997 SPE Annual Technical Conference and Exhibition, San Antonio, Oct. 5–8.
15. Land, C.S.: "Calculation of Imbibition Relative Permeability for Two- and Three Phase Flow From Rock Properties," *SPEJ* (June 1968) 149–56; *Trans.,* AIME, **243.**
16. Morrow, R. and Harris, C.C.: "Capillary Equilibrium in Porous Media," *SPEJ* (March 1965) 15–24.
17. Wardlaw, N.C. and Taylor, R.P.: "Mercury Capillary Pressure Curves and the Interpretation of Pore Structure and Capillary Behaviour in Reservoir Rocks," *Bull. Can. Pet. Geo.*, **24**, No. 2 (June 1976) 225–62.
18. Hammervold, W.L., Knutsen, Ø., Iversen, J.E., and Skjaeveland, S.M.: "Capillary Pressure Scanning Curves by the Micropore Membrane Technique," paper presented at the 1996 International Symposium on Evaluation of Reservoir Wettability and Its Effect on Oil Recovery, Montpellier, France, Sept. 11–13; revised version to appear in *J. Pet. Sci. & Eng*.
19. Topp, G.C. and Miller, E.E.: "Hysteretic Moisture Characteristics and Hydraulic Conductivities for Glass-Bead Media," *Soil Sci. Soc. Amer. Proc.* (1966) **30,** 156–162.
20. Colonna, J., Brissaud, F., and Millet, J.L.: "Evolution of Capillarity and Relative Permeability Hysteresis," *SPEJ* (Feb. 1972) 28–38; *Trans.,* AIME, **253.**
21. Burdine, N.T.: "Relative Permeability Calculations From Pore Size Distribution Data," *Trans.* AIME (1953) **198,** 71–77.
22. Braun, E.M. and Holland, R.F.: "Relative Permeability Hysteresis: Laboratory Measurements and a Conceptual Model," *SPERE* (Aug. 1995) 222–28.

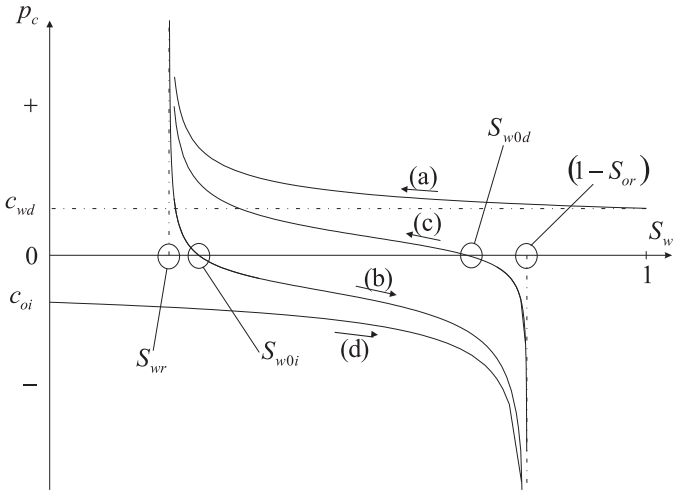

Fig. 1—Schematic of bounding curves: (a) primary drainage; (b) (secondary) imbibition; (c) secondary drainage; (d) primary imbibition.

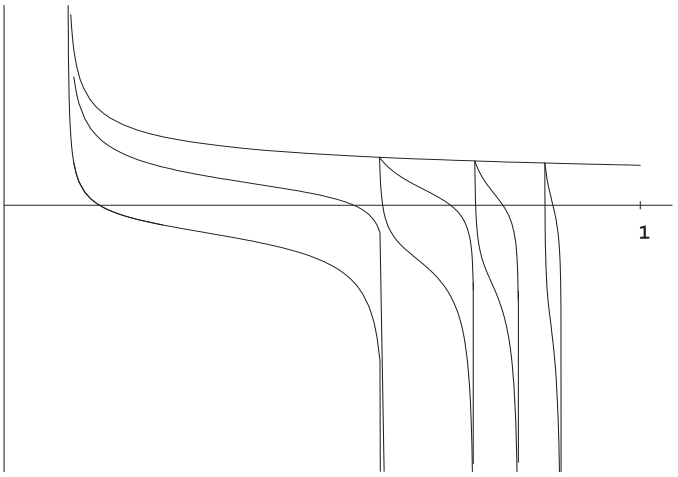

Fig. 2—Scanning loops with first reversal on the primary drainage curve and second reversal at the respective residual oil saturation.

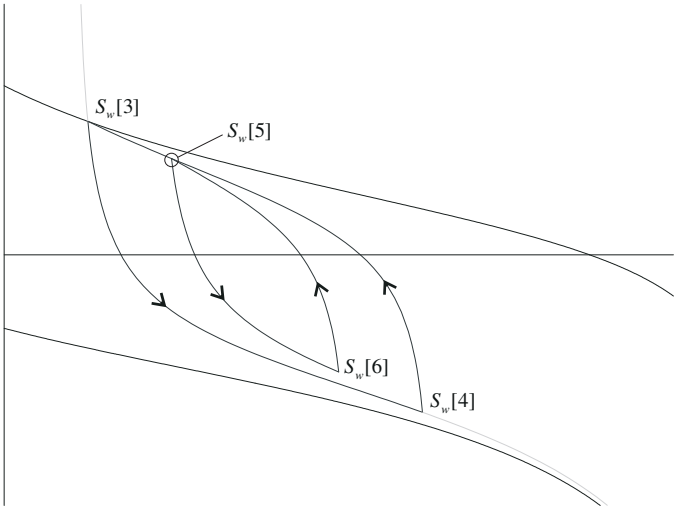

Fig. 3—A family of scanning loops spawned from a reversal point on the secondary drainage bounding curve.

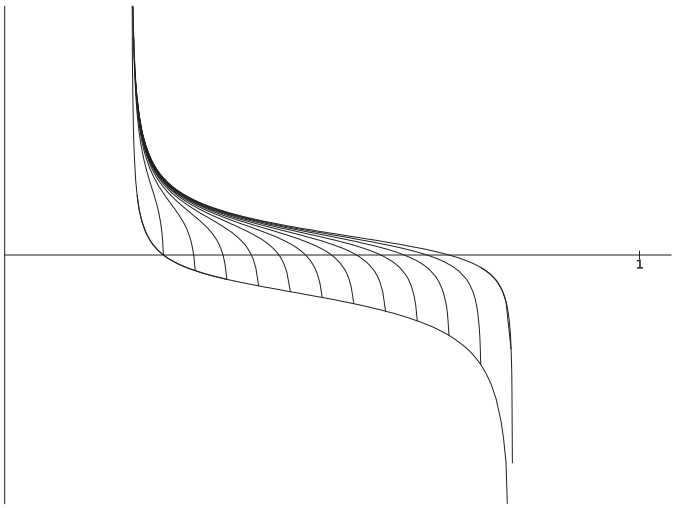

Fig. 4—Series of drainage scanning curves initiated at different reversal points on the imbibition bounding curve.

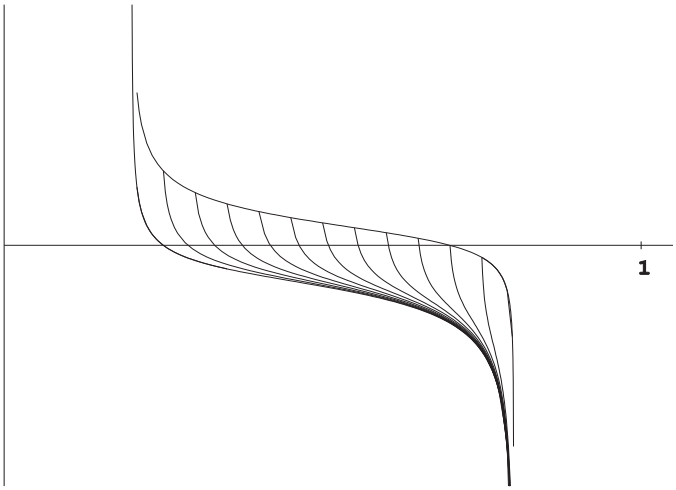

Fig. 5—Series of imbibition scanning curves initiated at different reversal points on the secondary drainage bounding curve.

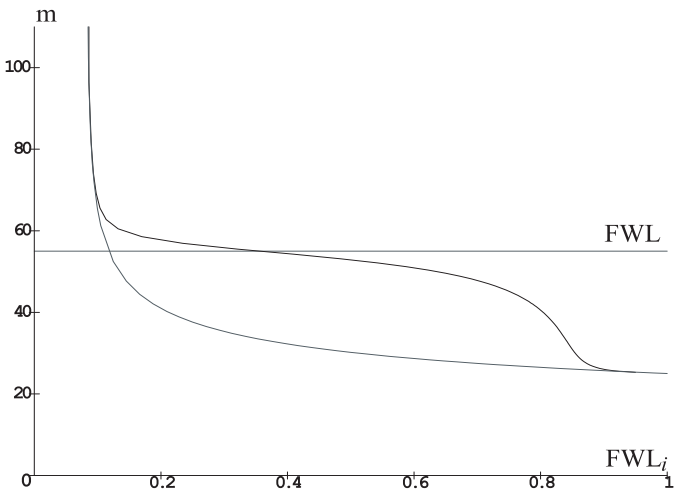

Fig. 6—Height above free water level (FWL) as a function of water saturation for two values of FWL; transition from a primary drainage curve at FWL$_i$ over to an imbibition dominated curve at FWL.

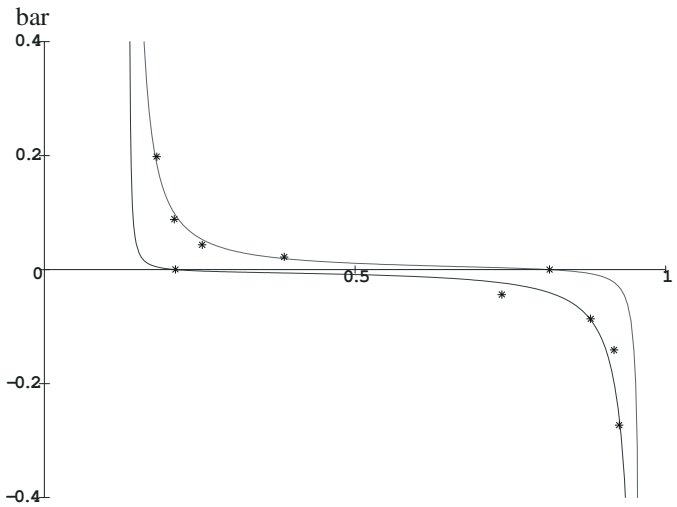

Fig. 7—Capillary pressure correlation fitted to forced imbibition and forced drainage centrifuge data from special core analysis.

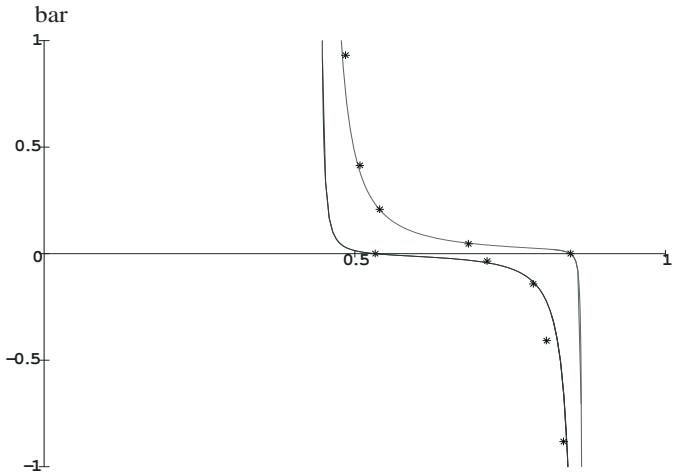

Fig. 8—Capillary pressure correlation fitted to forced imbibition and forced drainage centrifuge data for another core.

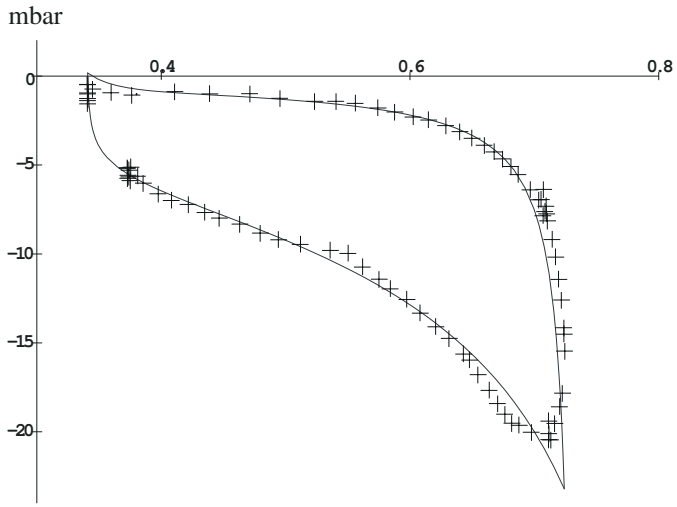

Fig. 9—Capillary pressure correlation fitted to the large scanning loop data.

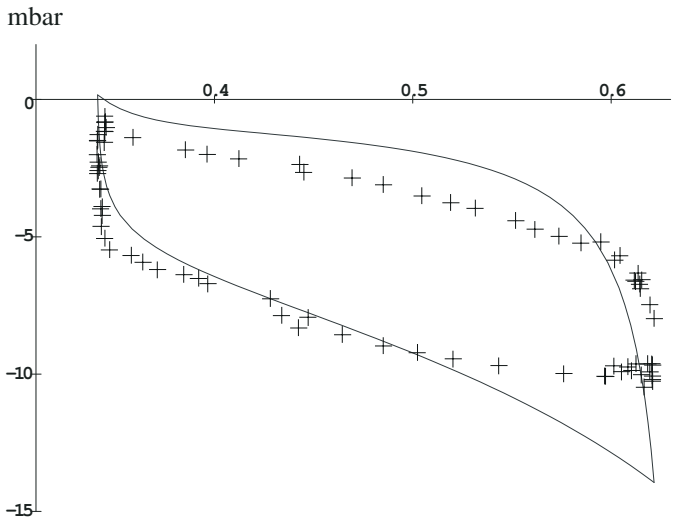

Fig. 10—Predicted medium scanning loop and measured data.

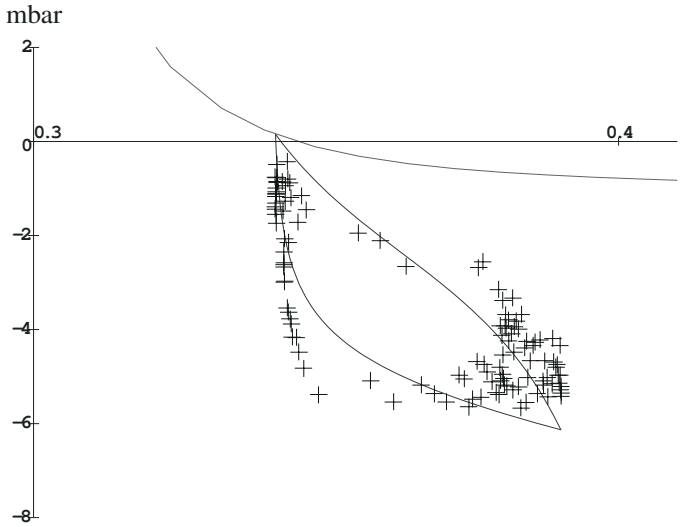

Fig. 11—Predicted small scanning loop and measured data.

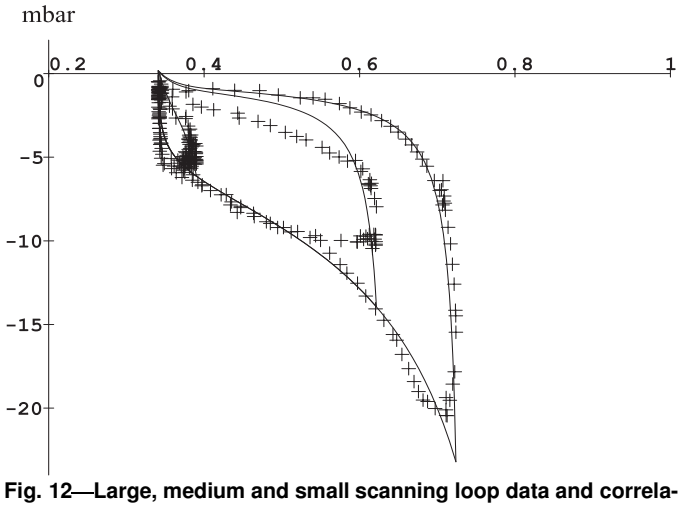

Fig. 12—Large, medium and small scanning loop data and correlation curves shown together.

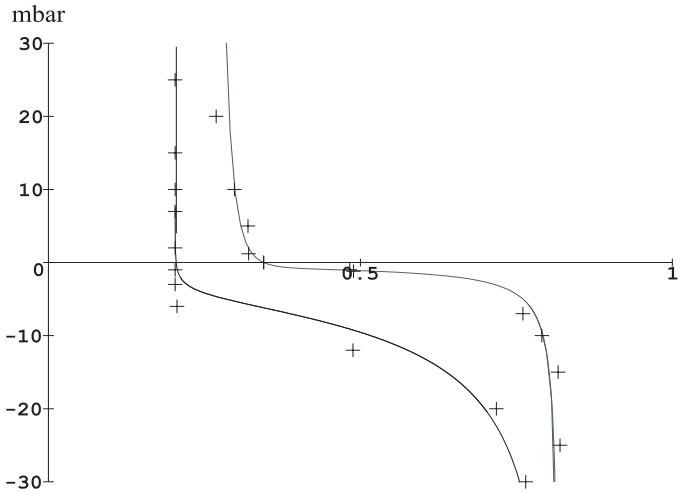

Fig. 13—Predicted bounding curves and measured data.

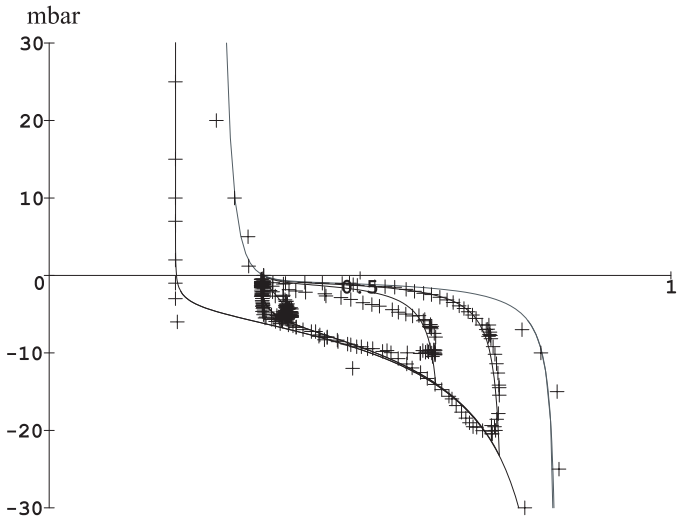

Fig. 14—All data and fitted curves shown together.

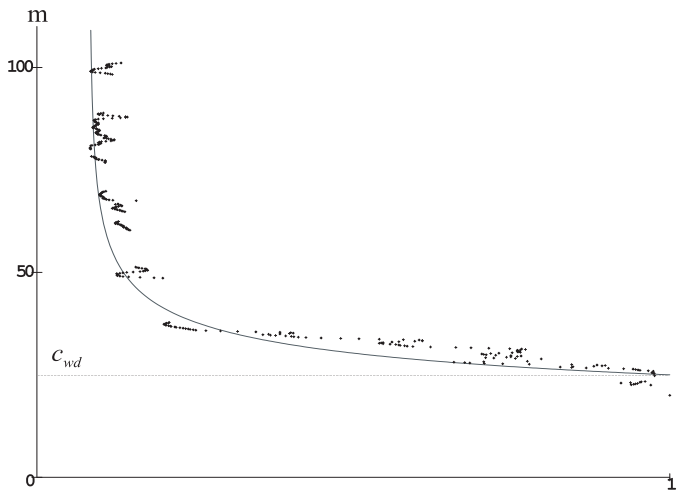

Fig. 15—Height above the free water level as a function of water saturation, well data and fitted correlation, initial conditions, primary drainage.

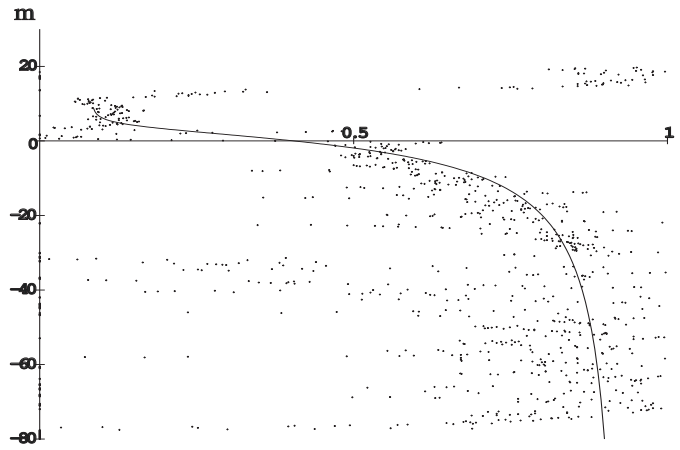

Fig. 16—Height above the free water level in 1994 as a function of water saturation, well data and fitted correlation, imbibition bounding curve.

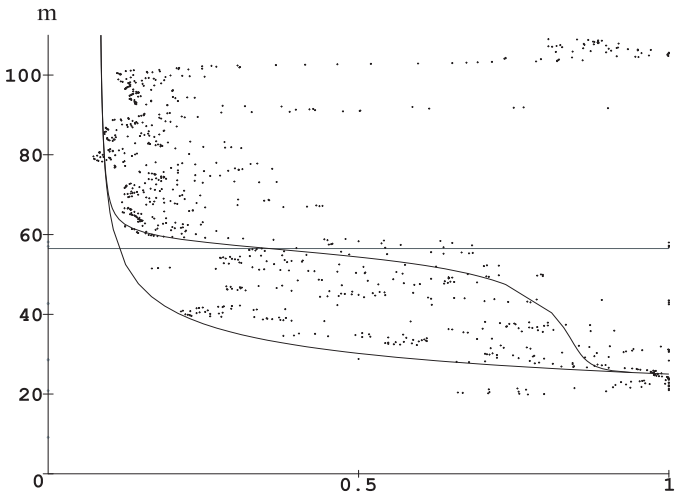

Fig. 17—Height above the free water level in 1992 as a function of water saturation, well data and prediction by correlation, transition from primary drainage to imbibition bounding curve.

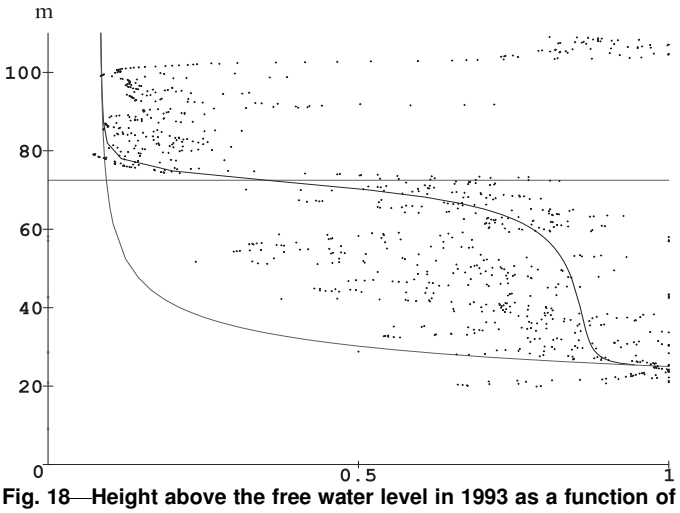

Fig. 18—Height above the free water level in 1993 as a function of water saturation, well data and prediction by correlation, transition from primary drainage to imbibition bounding curve.

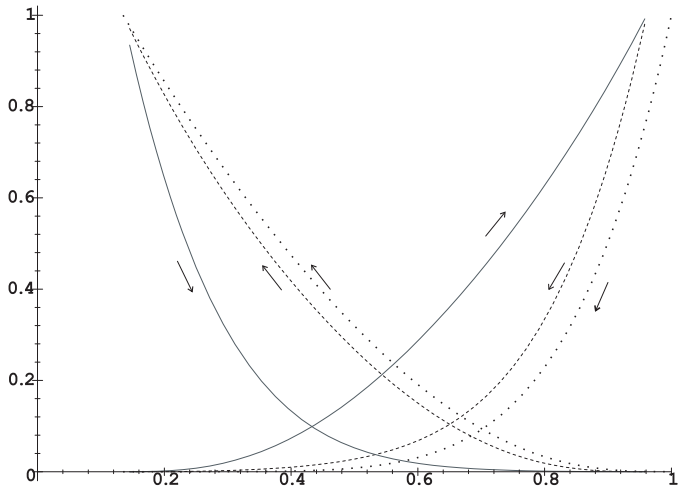

Fig. 19—Relative permeability curves for primary drainage, imbibition, and secondary drainage, data from Fig. 7.

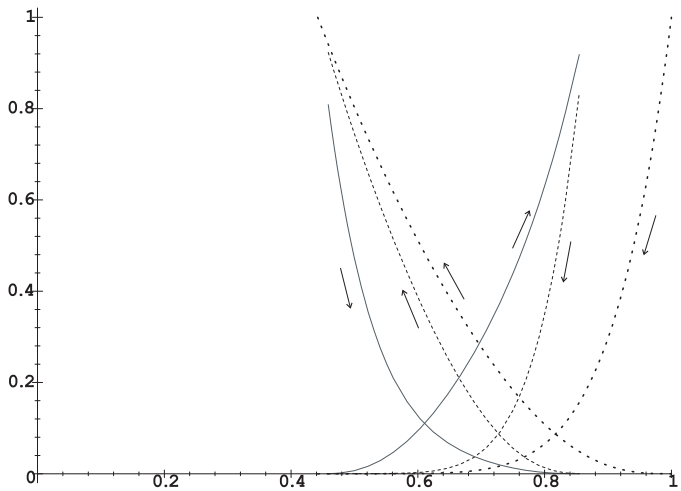

Fig. 20—Relative permeability curves for primary drainage, imbibition, and secondary drainage, data from Fig. 8.